PERGAMON

Carbon 41 (2003) 539–547

CARBON

Synthesis of carbon nanotubes over Fe catalyst on aluminium and suggested growth mechanism

C. Emmenegger[a,*], J.-M. Bonard[b], P. Mauron[a], P. Sudan[a], A. Lepora[c], B. Grobety[c], A. Züttel[a], L. Schlapbach[a]

[a]*Université de Fribourg, Département de Physique, Ch. du Musée 3, Pérolles, CH-1700 Fribourg, Switzerland*
[b]*Faculté des Sciences de Base, Ecole Polytechnique Fédérale de Lausanne, CH-1015 Lausanne, Switzerland*
[c]*Université de Fribourg, Département de Minéralogie et de Pétrographie, Pérolles, CH-1700 Fribourg, Switzerland*

Received 27 May 2002; accepted 11 October 2002

Abstract

Carbon nanotubes (CNTs) have been grown by the decomposition of C_2H_2 over a thin catalyst film in order to investigate the growth mechanism of CNTs by chemical vapour deposition (CVD). The catalyst was prepared from an iron nitrate precursor solution that was spin-coated on an aluminium substrate. The density (mg cm^{-2}) and the length of the CNTs were greatly influenced by the precursor concentration, the time of deposition, the temperature and the ratio of C_2H_2:N_2. Scanning and transmission electron microscopy, X-ray photoelectron spectroscopy and X-ray diffraction measurements have been carried out in order to investigate the behaviour of the catalyst before and during the growth process. The iron nitrate film formed an amorphous iron oxide layer that transformed to crystalline Fe_2O_3, which was reduced to Fe_3O_4 and FeO in contact with the C_2H_2: N_2 reaction atmosphere. The CNTs synthesis took place on small iron carbide (Fe_3C) particles that were formed from the FeO.

Keywords: A. Carbon nanotubes; B. Pyrolysis; C. Scanning electron microscopy, X-ray diffraction; D. Mechanical properties

1. Introduction

Since the original work of Iijima [1] in 1991, carbon nanotubes (CNTs) have been recognised to possess promising properties [2], in particular for applications in chemistry, physics and the area of nanotechnology. Indeed, CNTs have been used to build field-effect transistors [3], as one-dimensional quantum wires [4], as a hydrogen storage material [5–8] or as electron field emitters [9–11] for flat panel displays [12–14]. Due to their inherent stiffness, CNTs are mechanically resistant and can be used as probe tips for atomic force microscopy [15] and scanning tunnelling microscopy [16,17]. Another potential application that is currently under investigation is their use as electrode materials for electrochemical double layer capacitors (ECDL) [18,19], also called supercapacitor electrodes [20]. These supercapacitors require a large specific surface area, one of the main attributes of CNTs. Many techniques for the producing CNTs have been developed, using a variety of conditions, but relatively few studies have systematically investigated the growth mechanism of CNTs [21–23] or carbon fibres [24,25].

Our aim in the present work is to investigate the large-scale synthesis of CNTs produced by chemical vapour deposition (CVD) processes [26,27]. The effects of influential parameters such as temperature, iron nitrate concentration, the deposition time and hydrocarbon flow rate were studied. Electron microscopy observations as well as X-Ray photoelectron spectroscopy and X-Ray diffraction measurements allow us to propose a growth model. Finally it is shown that the final CNT film morphology depends strongly on the method used to terminate the deposition process—either a high yield of

*Corresponding author. Tel.: +41-26-300-9101; fax: +41-26-300-9747.
E-mail address: christophe.emmenegger@unifr.ch (C. Emmenegger).

0008-6223/02/$ – see front matter
PII: S0008-6223(02)00362-7

randomly entangled CNTs [28] or well-aligned CNTs with an amorphous carbon (a-C) cover layer [29] may be produced.

2. Experimental

The aluminium substrates (20 cm^2 area) are coated with an ethanolic solution of iron nitrate ($Fe(NO_3)_3 \cdot 9H_2O$) by spin coating, which leads to a very homogeneous Fe-containing film. The coated aluminium substrate is then mounted on a stainless steel support and inserted into a quartz tube furnace. The furnace is purged with 1000 sccm N_2 for 5 min before heating up to the deposition temperature. Subsequently, a mixture of 2–6 sccm (0.4–1.2%) C_2H_2 and 500 sccm N_2 is introduced at 1 bar for 15–180 min. The temperature of the substrate is varied between 600 and 650 °C, the upper limit being determined by the melting point of the aluminium at 660 °C. Deposition was terminated in one of two ways: the furnace was either purged with 500 sccm N_2 for 5 min and then evacuated, or simply evacuated immediately without prior purging. Unless stated otherwise, the reference conditions are 65 min of growth in 1.2% of C_2H_2 at 650 °C.

In a first phase (Section 3.1), we consider the importance of the temperature (600–650 °C) on the CNT growth with 60 and 120 mM of iron nitrate and by stopping the deposition by directly pumping the reaction atmosphere.

In a second phase (Sections 3.2 and 3.3), we study the yield of CNTs at 650 °C as a function of iron nitrate concentration (1–240 mM) and time of deposition (65–270 min). The real density (mg cm^{-2}) of the films is estimated by weighting the substrate before and after the deposition. This allows us to assess the influence of deposition time and the iron nitrate concentration on the growth rate, as this parameter is directly related to the amount of synthesised CNTs.

Morphological analysis is performed with a Jeol 6300 F scanning electron microscope (SEM) operating at 5 kV, as well as with a Philips EM 430 high-resolution transmission electron microscope (TEM) operating at 300 kV. X-ray photoelectron spectroscopy (XPS), excited with Mg Kα ($h\nu$=1253.6 eV) radiation in a UHV chamber at a low pressure ($<2\times10^{-8}$ mbar), is used to study and characterise the surface composition of the substrate. To characterise the initial phase of the growth with the different chemical transformations of the catalyst, SEM and XPS is carried out on aluminium substrates coated with different iron nitrate concentrations from 1 to 240 mM and heated at 650 °C during 20 min in the CVD system under a pure N_2 atmosphere. Finally, in situ X-ray diffraction measurements are performed at the growth temperature under C_2H_2 atmosphere follow the transformations of the catalyst layer. The measurements and experiments details will be given in a forthcoming paper [30].

3. Results and discussion

3.1. Produced carbon nanostructures

We examine in this section the range of parameters which allows to obtain CNTs. SEM observations show at 600 °C (Fig. 1a) an abundance of impurities like a-C that forms a rough surface without any CNTs. Indeed, this temperature is not high enough to modify the morphology [30] and the chemistry of the catalyst and hence to favour the synthesis of graphitic elements. Increasing the temperature to 625 °C produces randomly aligned nanotubes, as in Fig. 1b, and the CNTs yield becomes much higher at 650 °C (Fig. 1c). At 650 °C, randomly entangled CNTs are obtained for 60 and 120 mM, while the measured amount of CNTs is four times as large with on 120 mM as compared with 60 mM (see also Eq. (1)). The length of the CNTs also increases with the temperature between 625 and 650 °C, reaching a maximum value between 20 and 30 μm.

SEM observations reveal also that a sufficient flow of C_2H_2 (1.2%, Fig. 1c) has to be introduced in our reactor to maximise the yield of CNTs, as shown on Fig. 2 for hydrocarbon flows between 0.4 to 1.2%. With 0.4% of C_2H_2, only impurities like a-C mixed with iron carbide are grown (Fig. 2a), whereas with 0.8% of C_2H_2 carbon filaments with a-C and few CNTs are synthesised (Fig. 2b). This shows the importance to have a precise ratio between the inert (98.8%) and the hydrocarbon (1.2%) gases in order to synthesise a large amount of CNTs without impurities (Fig. 2c). Similar behaviour is observed at precursor concentrations of 60 and 150 mM.

The CNTs produced with iron concentration between 20 and 240 mM are principally MWNTs, as shown in the TEM micrograph of Fig. 3. For each catalyst concentration the size of the CNTs is rather uniform. Their diameter measured with SEM varies between 10 and 40 nm with the smaller diameter corresponding to the smallest efficient iron nitrate concentration (20 mM). The length of the CNTs as measured by SEM varies between 2.5 and 30 μm depending on the precursor concentration (from 2.5 to 5 μm with 20–30 mM and up to 30 μm with 120 mM of iron nitrate).

SEM observations carried out on the substrate surfaces coated with different iron nitrate concentrations do not reveal any formation of clusters. No cluster or metal particles are found for low concentrations (1–20 mM) but a rough film of iron oxide (Fig. 4a,b) forms without any distinguishable features. However, the surface roughness becomes more significant and homogeneous for the iron nitrate concentrations higher than 30 mM as small hills and cracks form on the surface. XPS measurements show that an iron oxide layer completely coats the surface from 30 mM up, whereas the iron oxide layer covers only partly the surface with smaller catalyst concentrations (Fig. 5).

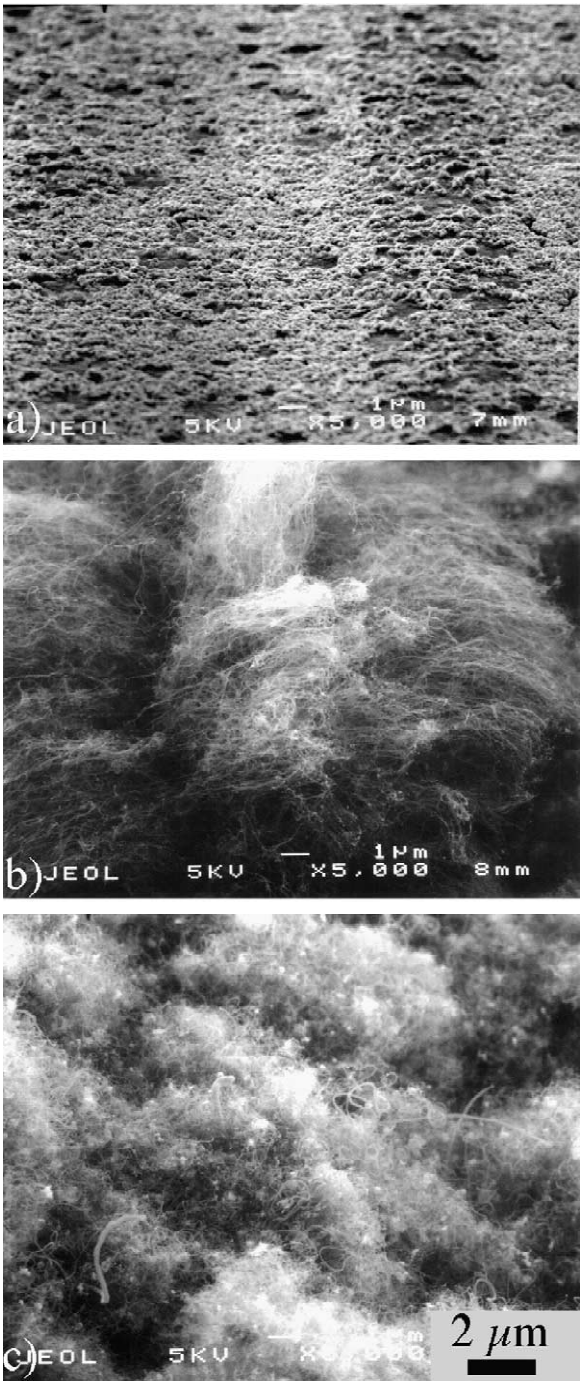

Fig. 1. SEM micrographs of CNTs grown at temperatures of (a) 600, (b) 625, and (c) 650 °C with 120 mM of iron nitrate during 65 min. The growth has been terminated by direct pumping. Micrographs a–c have been taken at the same magnification.

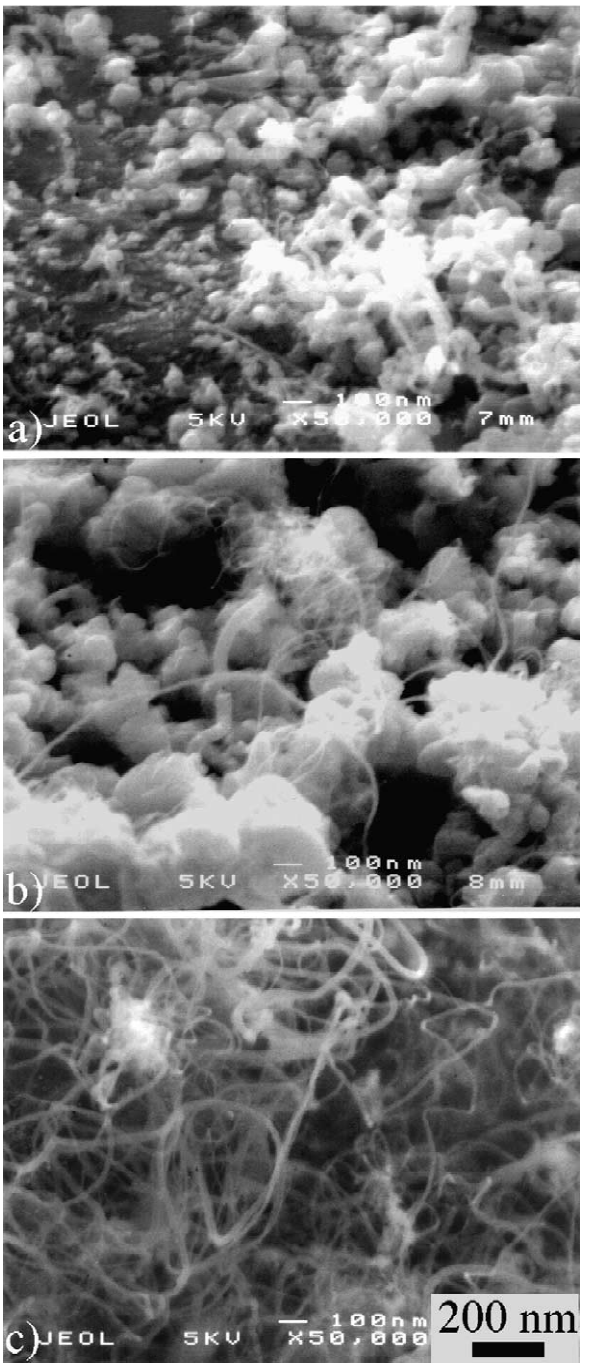

Fig. 2. SEM micrographs of CNTs grown with (a) 0.4, (b) 0.8, and (c) 1.2% of C_2H_2 with 120 mM of iron nitrate during 65 min. The growth has been terminated by direct pumping. Micrographs a–c have been taken at the same magnification.

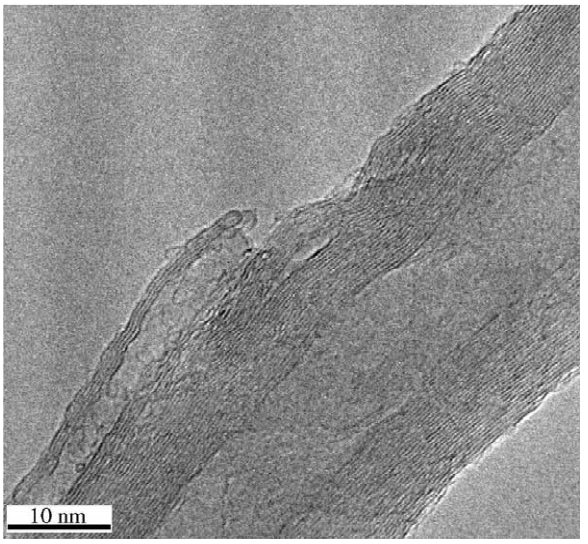

Fig. 3. TEM micrograph of a MWNT produced at 650 °C with 120 mM of iron nitrate during 65 min.

Indeed, Fig. 5 shows clearly that from 30 mM the Al(2p–2s) peaks intensity decreases strongly whereas the iron and iron oxide peaks intensity increase significantly.

3.2. Yield of CNT growth

SEM observations and CNT yield measurements show that deposition time longer than 65 min and iron nitrate concentrations higher than 120 mM do not influence significantly the CNT density (mg cm^{-2}). These first results allow us to focus our investigations on smaller iron nitrate concentrations and shorter times of deposition. For all depositions carried out during 65 min with concentrations below 20 mM (Fig. 4a,b), the homogeneous catalyst film transforms into an irregular rough surface where no CNTs are synthesised. The CNT growth is very sparse at 20 mM (Fig. 4c,d) and a very small density of randomly aligned CNTs is obtained from 30 mM up to 60 mM. On the order hand, a very homogeneous growth of well-aligned CNTs (Fig. 4e,f) is achieved from 60 mM up to 240 mM with an a-C layer that caps the top of the CNTs from 120 mM on (Fig. 4e,f). A method to remove this impurity layer will be discussed in Section 3.2.

The CNT density (mg cm^{-2}) (shown in Fig. 6 as a function of iron nitrate concentration and time of deposition) is measurable only at iron nitrate concentrations larger than 20 mM. The CNT amount increases linearly from 20 mM up to 120 mM and reaches after 65 min the maximum value of 0.28 mg cm^{-2}. The amount of synthesised CNTs does not increase and saturates at iron nitrate concentrations larger than of 120 mM. The experimental behaviour of the CNT density can be represented with Eq. (1):

$$\rho(conc)\,[\mathrm{mg\,cm^{-12}}] = \frac{\rho_{\max}}{1+\exp\left[-\left(\frac{conc-93\,\mathrm{mM}}{21\,\mathrm{mM}}\right)\right]} \quad (1)$$

where *conc* is the iron nitrate concentration applied on the substrate, $\rho_{\max} = 0.28$ mg cm^{-2} is the maximal average CNT density measured on the sample, and 21 and 93 mM are the calculated concentration of the precursor corresponding to the minimum needed to measure a CNT density and to half the maximal density of synthesised CNTs, respectively.

3.3. Rate of nanotube growth

A large amount of impurities like a-C forms during the first 15 min and with iron nitrate concentrations below 60 mM, whereas carbon filaments mixed with a-C are synthesised with 120 and 150 mM. Randomly entangled CNTs are observed only from 30 min on for iron concentrations between 30 and 60 mM, and above 60 mM aligned CNTs coated with an a-C layer are synthesised. The CNT density begins to increase significantly only after 30 min of deposition and reaches the maximum value $\rho_{\max}$ after 65 min. The length increased also from 30 min of deposition on and reaches a maximum value of 30 μm after 65 min.

The experimental dependence of the CNT density on the iron nitrate concentration influence (previous section) and on the deposition time, can be expressed by Eq. (2), which was used to draw the three dimensional plot presented in Fig. 2:

$$\rho(conc)\,[\mathrm{mg\,cm^{-2}}] = 0.28 \cdot \frac{1}{1+\exp\left[-\left(\frac{conc-93\,\mathrm{mM}}{21\,\mathrm{mM}}\right)\right]} \cdot \frac{1}{1+\exp\left[-\frac{(t-37\,\mathrm{min})}{10\,\mathrm{min}}\right]} \quad (2)$$

The highest density is obtained with very compact films of well-aligned CNTs that grow preferentially perpendicular to the substrate (Fig. 4f). A compact a-C layer (Fig. 4e,f) forms at the top of the well-aligned CNTs when the reactor is purged with 500 sccm of N_2 at the end of the deposition. In this case, the residual C_2H_2 volume in the reactor diminishes exponentially with time, depending on the reaction velocity of residual CNT synthesis or of graphite activity (Fig. 2b). This implies that CNTs are still synthesised at the beginning of the purging. Impurities like a-C are produced when the C_2H_2 concentration decreases below the value necessary to sustain CNT growth (Section 3.3) (Fig. 2a), which produces a compact layer on the synthesised CNTs (Fig. 4f).

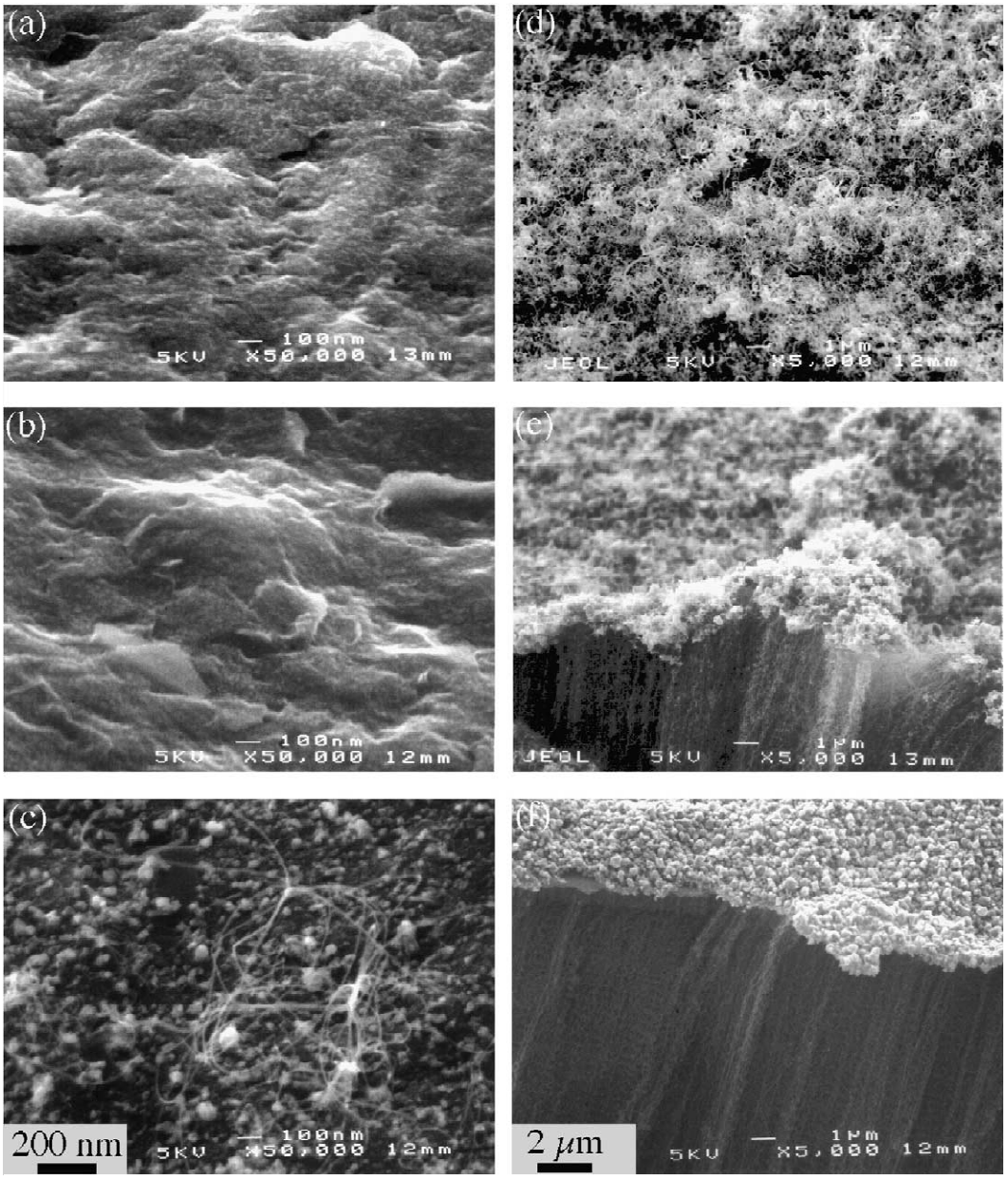

Fig. 4. SEM micrographs of CNTs grown with iron nitrate concentrations of (a) 1, (b) 5, (c) 20, (d) 60, (e) 150, and (f) 240 mM at 650 °C for 65 min. The growth has been terminated by purging the reactor with N_2. Micrographs a–c and d–f have been taken at the same magnification.

We can proceed in two different ways to avoid the formation of this a-C layer that caps the CNTs at concentrations higher than 120 mM. Firstly, we use an oxygen plasma treatment (400 W during 15 min with 5 ml min^{-1} of O_2 at a pressure of 0.003 mbar) in order to remove to a great extent the contaminating a-C layer. Secondly, we evacuate directly the reaction atmosphere at the end of the deposition instead of purging the furnace with 500 sccm of N_2 during the last 5 min. This process allows us to produce high yield of randomly entangled CNTs (Fig. 2c).

3.4. Growth mechanism

Many parameters, including the catalyst concentration, the temperature, the growth time, the gas composition and flow rate affect the nature of the carbon species in the final

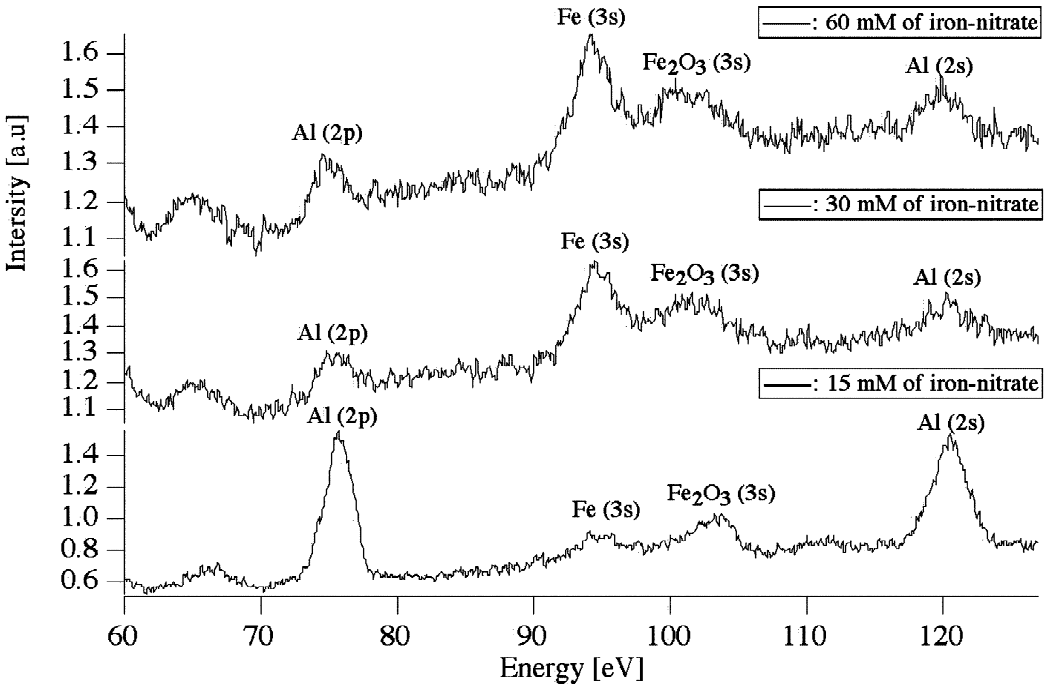

Fig. 5. XPS survey spectra acquired on Al substrates coated with 15, 30 and 60 mM of iron nitrate and heated at 650 °C during 30 min.

material [31]. The shape and size of the catalyst appears to play a key role. Oberlin et al. [32] observed that growth of thin primary fibres was due to a catalytic mechanism initiated by very small iron oxide particles that were reduced in pure iron by the presence of hydrogen in the furnace. Some authors claim that the active catalyst could be an iron carbide such as Fe_7C_3 [33], FeC [32] or Fe_3C [34]. In order to explain the central cavity in the fibres, Boehm et al. [34] assumed that the carbon layers might only nucleate on a specific face of the carbide crystals. Baker et al. [35] reported that nanofibres are obtained from large Fe particles (>20 nm) similar to liquid droplets. They suggested that acetylene decomposes on the exposed front surface of the metal particles in order to release hydrogen and carbon, which dissolves in the particle. The carbon then diffuses through the particle to form the body of the filament on the rear face of the metallic droplet. Recently Baker et al. [36] observed that CNTs were formed with the aid of smaller particles (<20 nm).

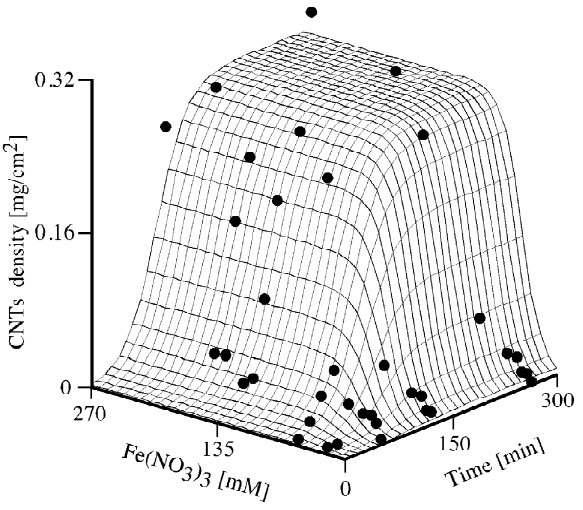

Fig. 6. Measured (circles) and calculated (Eq. (2)) CNT density as a function of iron nitrate concentration and time of deposition.

However, in the present study it was found that the iron nitrate solution deposited on the aluminium substrate formed a continuous layer and not individual particles, as shown on Fig. 8a where the suggested growth mechanism is schematised. XPS and XRD measurements show that for concentrations above 30 mM the iron nitrate decomposes completely to a continuous amorphous iron oxide film, whereas for lower concentrations some residual iron nitrate precursor is still detected (Fig. 5).

In situ high temperature X-ray measurements (Fig. 8) [30] reveal that the iron oxide layer transforms to a crystalline Fe_2O_3 ($\pm Fe_3O_4$) film during heating under nitrogen (Fig. 7a,b). Fragmentation of the film and the formation of smaller particles occurred after acetylene was introduced into the reaction chamber (Fig. 7b, see Figs. 4c and 6a,b). The hematite crystals are reduced to intermediate oxides (magnetite Fe_3O_4, wuestite FeO) by the hydrogen released from the pyrolysis of the acetylene (Fig.

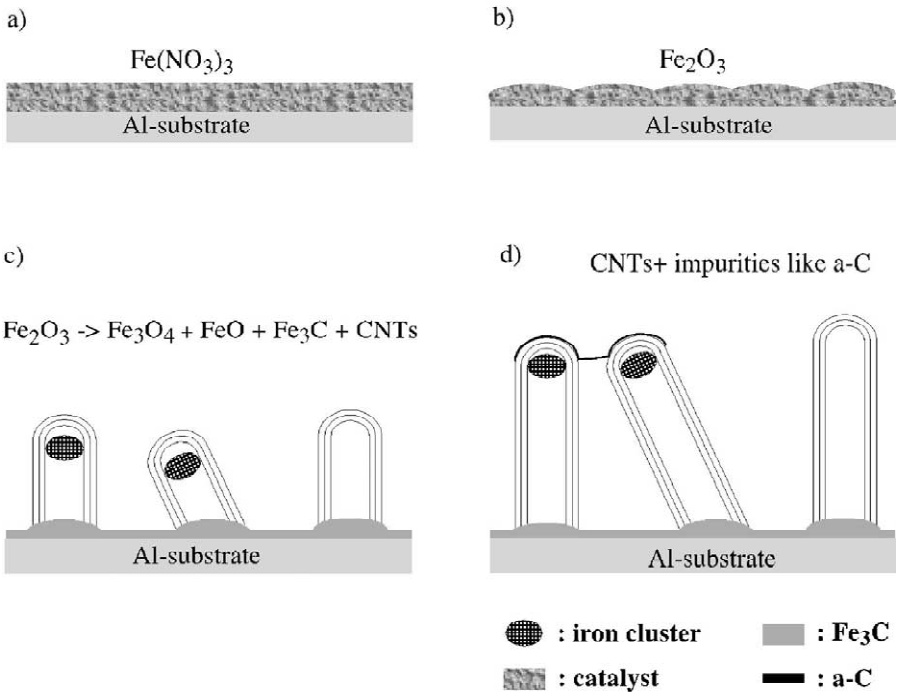

Fig. 7. Suggested CNT growth mechanism (see text, Section 3.4).

8, lower trace). Wuestite is finally transformed to (metastable) Fe_3C. The reduction process is accompanied by a large volume decrease of the solids inducing fragmentation of the catalyst layer. The delay of 30 min between the introduction of the hydrocarbon gas and the onset of growth can be explained by the kinetics of the reduction process [30]. Particles with diameters under 20 nm occur only several min after the onset of the reduction process. CNTs growth is, therefore, slow at the beginning. Graphite layers encapsulate some of the carbide particles before they reach the critical dimension and they are inactivated as possible nucleation sites.

The increase in the iron nitrate concentration results in a thicker layer. The fragmentation of such a layer produces a larger number of potential nucleation sites however CNTs formation is restricted to particles formed close to the surface. Therefore, the number of nucleation sites can therefore not be the only parameter responsible for the observed increase in CNT density with increasing nitrate concentration. The increase in density is also the result of increasing tube length with increasing nitrate concentration. In order to explain this, one has to remember that the catalyst does not only serve as nucleation sites, but also promotes the pyrolysis of acetylene. The surface of the particles that are encapsulated or taken up as nucleation sites for CNTs, are not accessible to the acetylene molecules and are not available for the pyrolysis reaction. In a thicker layer, the reduction process takes longer thus producing new surfaces, which are available for a longer time. There are also enough particles formed away from the surface, which can serve for the promotion of the acetylene pyrolysis. The asymptotic behaviour of the CNT density for solution concentrations above 150 mM (Fig. 2), e.g. the very slow growth for tubes longer than 30 μm, may be due to the increase of the diffusion path for acetylene molecules across the CNT layer down to the iron carbide layer. The CNTs already produced form a diffusion barrier between the gas stream and the catalyst layer. The importance of having enough active surfaces for catalysing the pyrolysis has been shown in low temperature CVD experiments (500–550 °C) using Co–Ni particles as nucleation sites. Without adding platinoids, which do not act as nucleation sites but are strongly catalysing the acetylene breakdown, no CNTs are observed [37]. Similar observations are made in pyrolysis reactors, where periodic decoking and regeneration of the catalyst is necessary [38].

A second transformation within the catalyst layer has been observed in situ X-ray experiments. After 20–30 min of exposure to the acetylene–nitrogen atmosphere, the iron carbide starts to decompose into metallic iron and graphite [30], a process known as dusting in steel making industry [39] (Fig. 1, upper trace). This reaction is also accompanied by a decrease in solid volume and contributes to the reduction in grain size. The onset of dusting observed in the in situ XRD experiments coincides with the steep increase in CNT production observed in the present CVD experiments.

The parallel growth of the tubes only observed in

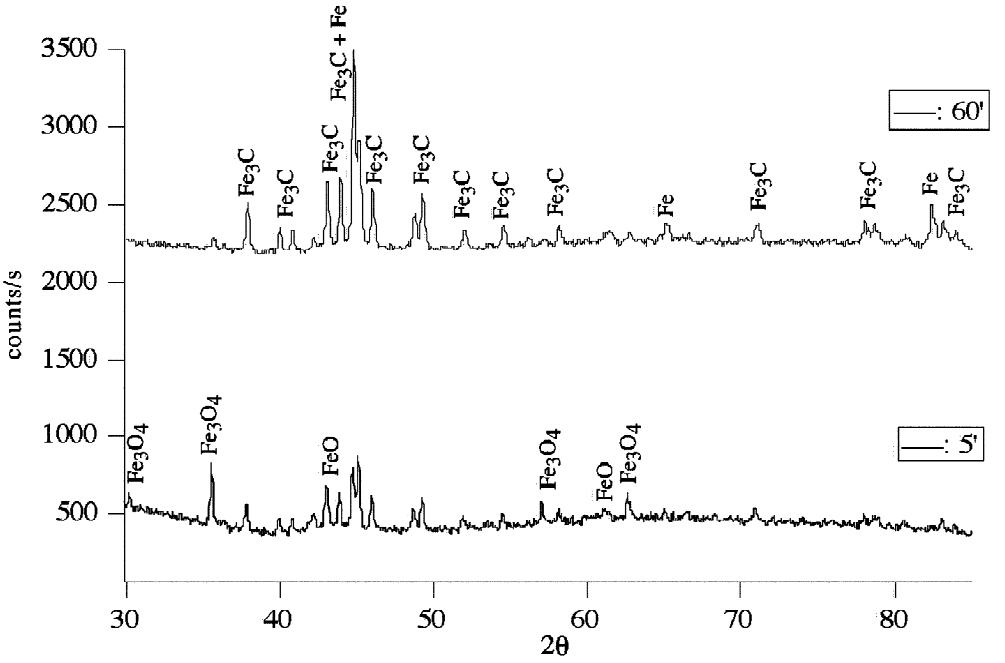

Fig. 8. In situ powder X-ray diffraction patterns acquired at 650 °C after 5 min (lower trace) and 60 min (upper trace) exposure to C_2H_2 on a glass substrate with 60 mM of iron nitrate. Both samples still contain some oxide remnants [30].

experiments with high concentrations may be explained by steric hindrance. A high number of nucleation sites leads to a high density of simultaneously growing CNTs, with the only unimpeded growth direction for the latter being perpendicular to the substrate.

Iron carbide clusters can be observed at the base as well as at the tip of the CNTs. The nucleation of the CNTs appears to occur at both the free surface of the particles (base growth) as well as at the interface between particles and substrate or between particles (top growth) (Fig. 7c,d). The alignment of the CNTs is only maintained when nitrogen is introduced into the chamber at the end of the synthesis runs. The nitrogen dilutes the concentration of acetylene and produces an amorphous deposit similar to those obtained using low acetylene concentrations during the full duration of the synthesis (see Fig. 2a). Under these conditions carbon is deposited as an amorphous layer onto the substrate, similar to the layer observed on top of the aligned CNTs after the nitrogen treatment. The amorphous deposit stabilises the previously deposited CNT 'garden'—without it subsequent evacuation of the reaction chamber pumping seems to destroy the CNT alignment.

4. Conclusions

Our CNTs growth study, which has explored the most important parameters of the CVD process, has clearly demonstrated that CNTs grow in a wide range of deposition conditions. But the largest CNT density can be obtained only by controlling precisely parameters such as the time of deposition, the temperature and the iron nitrate concentration. Furthermore, the observations of the catalyst behaviour carried out with SEM, XPS and X-ray diffraction allow us to suggest a growth mechanism. It turns out that the catalyst did not form distinct clusters but a rough film of Fe_2O_3, coating uniformly the surface of the substrate for concentrations higher than 30 mM, that transformed into Fe_3O_4, FeO and Fe_3C following the introduction of C_2H_2. After 20 to 30 min of exposure to the acetylene–nitrogen atmosphere, the iron carbide started to decompose into Fe and graphite, this process coinciding with the onset of CNT growth. TEM and SEM observations allowed to conclude that the CNTs were synthesised on iron carbide clusters.

Acknowledgements

We would like to thank the Centre Interdépartemental de Microscopie Electronique of the Ecole Polytechnique Fédérale de Lausanne for access to scanning and transmission electron microscopes. Ch. Neururer, F. Bourqui, and the mechanical workshop under the leadership of E. Mooser and O. Raetzo provided excellent technical assistance. The financial support of the project by the Swiss CTI (Commission for Innovation and Technology) is acknowledged.

References

[1] Iijima S. Nature 1991;354(6348):56–8.
[2] Bernier P, Maser W, Journet C, Loiseau A, De la Chapelle ML, Lefrant S et al. Carbon 1998;36(5–6):675–80.
[3] Tans SJ, Verschueren ARM, Dekker C. Nature 1998;393(6680):49–52.
[4] Tans SJ, Devoret MH, Dai H, Thess A, Smalley RE, Geerligs LJ et al. Nature 1997;386(6624):474–7.
[5] Dillon AC, Jones KM, Bekkedahl TA, Kiang CH, Bethune DS, Heben MJ. Nature 1997;386(6623):377–9.
[6] Chahine R, Bose TK. Int J Hydrogen Energy 1999;19(2):161–4.
[7] Nützenadel Ch, Züttel A, Chartouni D, Schlapbach L. Electrochem Solid State Lett 1999;2(1):30–2.
[8] Züttel A, Sudan P, Mauron Ph, Kiyobayashi T, Emmenegger Ch, Schlapbach L. Int J Hydrogen Energy 2002;27(2):203–12.
[9] Rinzler AG, Hafner JH, Nikolaev P, Lou L, Kim SG, Tomanek D et al. Science 1995;269(5230):1550–3.
[10] de Heer WA, Châtelain A, Ugarte D. Science 1995;270(5239):1179–80.
[11] Bonard JM, Kind H, Stöckli Th, Nilsson LO. Solid State Electron 2001;45(6):893–914.
[12] Kind H, Bonard JM, Emmenegger Ch, Nilsson LO, Hernadi K, Maillard-Schaller E et al. Adv Mater 1999;15(11):1285–9.
[13] Fan S, Chapline MG, Franklin NR, Tombler TW, Cassel AM, Dai H. Science 1999;283(5401):512–4.
[14] Xie SS, Li WZ, Pan ZW, Chang BH, Sun LF. Eur Phys J D 1999;9(1–4):85–9.
[15] Hafner JH, Cheung CL, Oosterkamp TH, Lieber CM. J Phys Chem B 2001;105(4):743–6.
[16] Biro LP, Lazarescu S, Lambin P, Thiry PA, Fonseca A, Nagy B et al. Phys Rev B 1997;56(19):12490–8.
[17] Hafner JH, Cheung CL, Lieber CM. Nature 1999;398(6730):761–2.
[18] Morimoto T, Hiratsuka K, Sanada Y, Kurihara K. J Power Source 1996;60(2):239–47.
[19] Niu C, Sichel EK, Hoch R, Moy D, Tennent H. Appl Phys Lett 1997;70(11):1480–2.
[20] Mahon PJ, Paul GL, Keshishian SM, Vassalo AM. J Power Source 2000;91(1):68–76.
[21] Kind H, Bonard JM, Forrò L, Kern K, Hernadi K, Nilsson LO et al. Langmuir 2000;16(16):6367–73.
[22] Bandow S, Asaka S, Saito Y, Rao AM, Grigorian L, Richter E et al. Phys Rev Lett 1998;80(17):3779–82.
[23] Li DC, Dai L, Huang S, Mau AWH, Wang ZL. Chem Phys Lett 2000;316(5–6):349–55.
[24] Renshaw GD, Roscoe C, Walker PL. J Catal 1970;18(2):164–83.
[25] Tibbetts GG. J Cryst Growth 1984;66(3):632–8.
[26] Colomer JF, Stephan C, Lefrant S, Van Tendeloo G, Willems I, Konya Z et al. Chem Phys Lett 2000;317(1–2):83–9.
[27] Emmenegger C, Mauron P, Züttel A, Nützenadel C, Schneuwly A, Gallay R et al. Appl Surf Sci 2000;162–163(1–4):452–6.
[28] Gao Y, Liu J, Shi M, Elder SH, Virden JW. Appl Phys Lett 1999;74(24):3642–54.
[29] Küttel OM, Groening O, Emmenegger C, Schlapbach L. Appl Phys Lett 1998;73(15):2113–5.
[30] Lepora A, Métraux C, Grobety B, Emmenegger C, Züttel A. J Mater Res 2002: in press.
[31] Laurent C, Flahaut E, Peigney A, Rousset A. New J Chem 1998;22(11):1229–37.
[32] Oberlin A, Endo M, Koyama T. J Cryst Growth 1976;32(3):335–49.
[33] Ruston WR, Warzee M, Hennaut J, Waty J. Carbon 1969;7(1):47–57.
[34] Boehm HP. Carbon 1973;11(6):583–90.
[35] Baker RTK, Barber MA, Harris PS, Feates FS, Waite RJ. J Catal 1972;26(1):51–62.
[36] Baker RTK, Rodriguez NM. In: Materials Research Society Symposium Proceedings, Novel forms of carbon, vol. II, 1994, pp. 251–6.
[37] Coi YC, Shin YM, Lee YM, Lee BS, Park GS, Choi WB et al. Appl Phys Lett 2000;76(17):2367–9.
[38] Grabke HJ, Muller-Lorenz EM. Mater Corrosion 1998;49(5):321–7.
[39] Grabke HJ, Muller-Lorenz EM, Klower J, Agarwal DC. Mater Perform 1998;37(7):58–63.